2024 IEEE/RSJ International Conference on Intelligent Robots and Systems (IROS)
October 14-18, 2024. Abu Dhabi, UAE

Design Improvements to the Float Upper-Limb Exoskeleton Better Mimics the Glenohumeral Complex Kinematics

Giulia Bodo[1,2], Federico Tessari[3], Gianluca Capitta[2],
Luca De Guglielmo[2], Stefano Buccelli[2] and Matteo Laffranchi[2]

Abstract— **The shoulder glenohumeral complex stands out as one of the most complex structures within the human body. Designing a system that can effectively interface with it poses a significant challenge for researchers. In this study, we propose a methodology based on evaluating various metrics to assess the performance of new kinematic solutions for mimicking the glenohumeral complex. The proposed method is demonstrated on an existing design (Float) of an upper-limb exoskeleton. The results show a successful expansion of the reachable workspace and enhancement of the shoulder internal-external rotation. The improvements ensure the necessary range-of-motion for the patient's natural use of the exoskeleton. Specifically, the existing Eulerian wrist architecture is replaced with a 3-degree-of-freedom RPY wrist to better resemble the glenohumeral shoulder joint complex. This study also explores the trade-offs between these enhancements and the desired system manipulability.**

I. INTRODUCTION

Robot-assisted rehabilitation is emerging as a promising approach for aiding orthopaedic and neurological patients in regaining motor agency. Rehabilitating the upper limb necessitates the development of rehabilitative technologies that can accurately replicate the spatiotemporal motion patterns observed in the human body [1].

The human shoulder is known for its complexity, representing a challenge in designing robotic rehabilitation devices that can be coupled with it. This complexity implies that a single mechanical joint cannot fully replicate the nuanced motion of the shoulder complex. While literature provides a range of human kinematic models, many are overly simplistic in capturing the intricacies of human anatomy [2]. Models based on a dual-joint concept, such as the inner and outer shoulder joints, have been proposed to simulate the human workspace. However, relying solely on goniometric descriptions often falls short in fully characterizing the glenohumeral shoulder complex, particularly its diminishing functional capacity due to multiple movement restrictions across various joints and planes [3].

Active and passive degrees of freedom (DoFs) can be combined to enhance arm movements by adapting to the unique characteristics of the human anatomy [4][1]. As highlighted by Schiele et al. [5], two significant challenges arise: (i) to identify the exact location of human joints due to the intricate interactions between various articulations, acting around different axes and complex surface geometries; (ii) misalignment can occur due to slipping between the device and the limb, which is not inherently rigid.

The kinematic design must minimize the risk of collision and undesired motions, replicate the anatomical workspace, and guarantee a high manipulability [6] [7]. Moreover, ensuring proper alignment between anatomical and robotic joints is crucial for facilitating correct human-machine interaction and preventing patient's discomfort [8][9].

To address these challenges, different models were proposed [10][11][12]. They adopt approximations of the upper limb kinematic structure (i.e. location and number of degrees of freedom). The availability of upper-limb biomechanics models can guide the design process, minimizing misalignment between human and exoskeleton joints. Another complexity lies in emulating human redundancy, thus, the ability to reach the same pose in Cartesian space with different joint configurations. It is essential for the kinematic design to not restrict natural arm motion. Therefore, a viable approach involves relaxing the requirements on joint alignments in favor of kinematic structure. This can operate in parallel with the human body, taking in consideration the anthropometry of the interacting human limb without limiting its intrinsic redundancy. Over the past decade, several exoskeletons for upper limb rehabilitation were proposed (Float [13], Alex [14], Armeo [15], CleverArm [16] AnyExo [17], Harmony [18], Aramis[19]). Despite their significant differences, these devices share a common technological foundation: develop a solution that can be coupled with the human body, closely resembling the physiological movements of the shoulder and scapular complexes and that can exchange forces with the impaired limb.

The aim of this work is to propose an assessment methodology, including relevant metrics, to evaluate the capability of a mechatronic system to mimic physiological shoulder movements. In this study, the authors apply various evaluation metrics to two designs of the Float upper-limb exoskeleton. To demonstrate its potential in rehabilitative robotics, a new robotic prototype featuring a distinct kinematic configuration is showcased. The authors aim to prove that reworking the joint configuration of the Float exoskeleton [13] can: (i) achieve better coupling with the human body, (ii) expand the reachable workspace to enable patients to perform wider movements during rehabilitation sessions, (iii) enhance internal-external rotation movements, and (iv) provide in-

[1]PhD student in Mechanical Engineering at Politecnico di Torino, Torino, Corso Duca degli Abruzzi 24, 10129, Italy.

[2]Rehab Technologies Laboratory at Istituto Italiano Tecnologia, Genova, Via Morego 30, 16163, Italy.

[3]Postdoctoral Associate, Mechanical-Mechatronic Engineer The Eric P. and Evelyn E. Newman Laboratory for Biomechanics and Human Rehabilitation Department of Mechanical Engineering Massachusetts Institute of Technology.

sights for further kinematic design improvements.

II. MATERIALS AND METHODS

This study focuses on a 6-DoFs upper-limb exoskeletal prototype, designed at the IIT-INAIL-Rehab Technologies Lab, named Spherical Float [20]. With reference to Figure 1, J1, J2 allow scapular protraction/retraction and elevation/depression, J3, J4, J5 compose the spherical joint allowing glenohumeral movements and J6 allows elbow flexion/extension. The metrics considered for the kinematics structure design evaluation are: (i) size of reachable workspace surface, (ii) enhancement of the shoulder internal-external rotation, and (iv) evaluation of manipulability performances.

A. Size of reachable workspace, from Eulerian to RPY Wrist kinematic design

In the original Float shoulder model, an Eulerian wrist design was adopted. This solution, consisting of three rotational degrees of freedom, enables the rotation around three orthogonal axes that intersect each other in one common point (J3, J4, J5 axes with reference to Figure 2). The Eulerian wrist, depicted in Figure 2, is described using three angles (Euler angles) specifying consecutive rotations (e.g. z-x-z, x-y-x, y-z-y) about the coordinate axes. Despite achieving successful results [13], this design could not cover the entire physiological range (e.g., limited flexion and rotation movements). To broaden the reachable workspace and enhance overall maneuverability, a different kinematic structure was explored: a 3-DoF RPY wrist, shown in Figure 2. This design, similarly to the Eulerian wrist, can be described using three angles representing the orientation of the joint in a global coordinate system (Roll-Pitch-Yaw angles).

The design of a 3-DoF spherical joint can be approached using various kinematic structures. Depending on the location of the rotational joints in the spherical wrist, singularities may occur in different regions of the working area. The proposed redesign, which adopts the RPY wrist configuration, successfully relocates the gimbal lock away from typical working areas for humans (Table I).

Float	**Spherical Float**
• Resting Position (J3 above J5): human arm resting on the side of the trunk • Extended Flexion Movement (over 90°): human arm pointing orthogonally from the frontal plane	• Maximum extra-rotation: human arm trying to reach behind the neck • Maximum intra-rotation: human arm trying to reach the counter-lateral shoulder

TABLE I

GIMBAL LOCK CONFIGURATIONS FOR THE TWO ANALYZED DEVICES.

B. Manipulability evaluation

Manipulability can be used as indicator to improve the kinematics performances by changing the design of the device. By definition, manipulability is the capacity to change the end-effector pose (position and orientation) of a robotic device given a certain joint configuration. Manipulability can be defined with respect to the rotational Jacobian matrix and can be computed as the product of the singular values of the diagonal elements of the Sigma Matrix Σ, of the Jacobian singular value decomposition (UΣV) .

$$\mu = \Pi_{i-1}^{m}(\sigma_i), i = 1...n_{Joints} \tag{1}$$

The manipulability can range between zero and one; the higher it is, the easier it becomes to alter the end-effector pose within the analyzed configuration. The workspace under analysis has been delimited by constraining the obtainable yaw and roll angles to what can be physiologically performed by a human shoulder. Roll represents the glenohumeral internal-external rotation around the humerus axis, pitch represents the glenohumeral elevation rotation, and yaw represents the glenohumeral horizontal rotation along the azimuthal direction (as depicted in Figure 3). Referring to Figure 6, acceptable values pertain to configurations where the yaw angle value falls between -25° and 90°, and the roll angle value lies between -90° and 45°. These ranges were chosen to confine the analyzed area to internal-external rotations typical of simple activities of daily living (ADLs) movements.

C. Internal-external rotation performances

In the design using the Eulerian Wrist, the internal-external rotation movement was performed exploiting a single joint: Float J5 joint. In the RPY wrist kinematic structure, the internal-external rotation movement is achieved through a combined rotation of the three joints forming the spherical complex: Spherical Float J3-J4-J5 joints. To analyze how the two different design impact the internal-external movement, three successive rotations can describe a motion on the spherical surface, with reference to Figure 3: (I) Roll describes the intra-extra rotation around the humerus axes, (II) Pitch is the elevation movement, movement along the sphere meridians and (III) Yaw is the azimuthal movement along the sphere parallels.

D. Glenohumeral shoulder complex reachable workspace

To analyze the reachable workspace surface by the different spherical joint designs, it is possible to compute the flexion (θ) and abduction (Φ) angles achieved in various configurations. The workspace surface can be computed through a surface integral (considering , $\theta_{min}, \theta_{max} \in [0, 2\pi]$ and $\Phi_{min}, \Phi_{max} \in [0, \pi]$). Specifically, considering the shoulder joint as a spherical one, we could use, as a first approximation, a spherical surface integral.

$$A = \int_{\theta_{\min}}^{\theta_{\max}} \int_{\Phi_{\min}}^{\Phi_{\max}} R^2 \sin(\Phi) d\Phi d\theta \tag{2}$$

with

$$\theta_{min} \leq \theta \leq \theta_{max} \tag{3}$$

$$\Phi_{min} \leq \Phi \leq \Phi_{max} \tag{4}$$

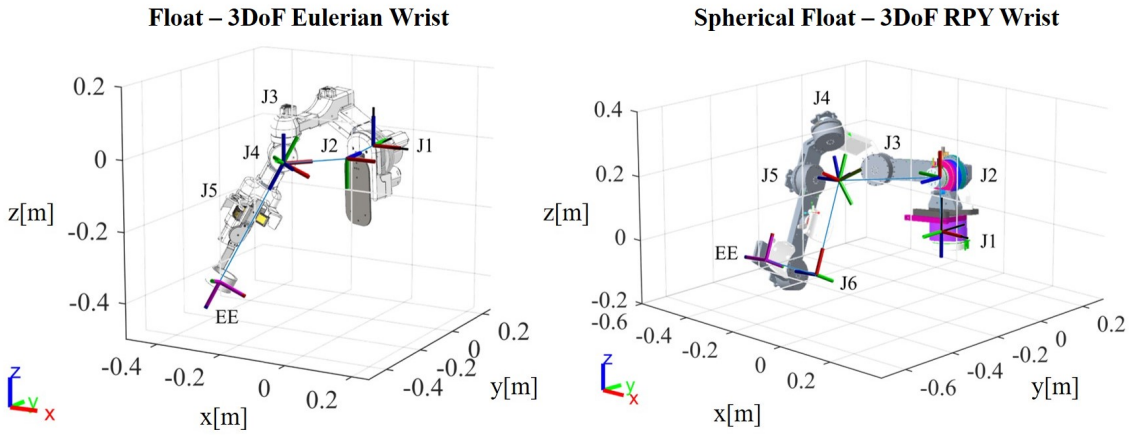

Fig. 1. Comparison between Float [13] and Spherical Float exoskeletons designed by Rehab Technologies Laboratory of Italian Insitute of Technology. In the figure are shown the rigid body trees of the compared kinematics. On the left Float is a 5 Dof device, the kinematic structure is characterized by the presence of an Eulerian wrist for the shoulder mobilization. The internal external rotation is performed exploiting J5 and the elbow flexion-extension is only passive (performed by the patient). On the other side, Spherical Float prototype is a 6-Dof device that exploits a RPY wrist complex for the shoulder mobilization using the combination of J3, J4, J5 to perform shoulder flexion-extension and abduction-adduction and internal-external rotation. The presence of J6, also, allows the active (performed by the exoskeleton) mobilization of the elbow.

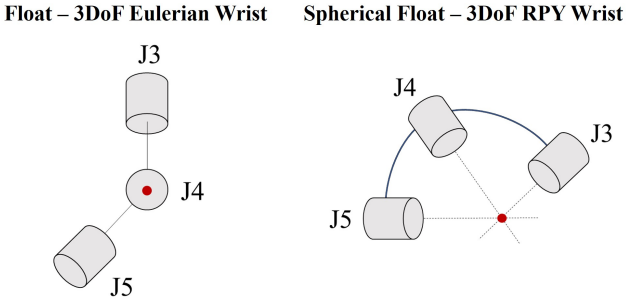

Fig. 2. In the 3-DOF Eulerian wrist solution, joint axes are positioned at 90° angles, offering simplicity but limited flexibility. The 3-DOF RPY wrist solution, on the other hand, features axes with angles of approximately 59° and 60°, providing a more versatile range of motion to mimic the complexities of the glenohumeral shoulder joint.

To determine the integration limits, an abduction-flexion graph is generated (see Figure 7). Due to the complexity of the relationship involved, the region is approximated by subdividing it into rectangles and performing the integral over these sub-regions (see Figure 8). Thus the overall area, considering n sub-regions, can be obtained as:

$$A_{\text{tot}} = \sum_{i=1}^{n} \int_{\theta_{\min_i}}^{\theta_{\max_i}} \int_{\Phi_{\min_i}}^{\Phi_{\max_i}} R^2 \sin(\Phi)\, d\Phi\, d\theta \qquad (5)$$

To assess the reachable workspace and musculoskeletal configurations more comprehensively, authors adopted a Vicon system [21] to measure the upper limb kinematic. This approach involves utilizing motion capture systems based on cameras, markers, and bio-mechanical models. Three markers were placed at sternum (ST marker), shoulder (SH marker) and elbow (EL marker) level (Figure 4) of a healthy individual used as anthropometric reference.

The subject was asked to cover the reachable range of motion possibly not involving the scapular joint (thus to involve just the glenohumeral complex). From the marker data, it is possible to determine the segments sternum-shoulder and shoulder-elbow, as well as the rotation frame applicable at the shoulder center. Consequently, the angles of flexion and abduction can be derived, and the calculation of the covered area can be performed according to Equation 5. These acquisitions allowed for comparisons with the kinematics structure proposed by the two spherical joint models, providing valuable insights into the effectiveness of the new joint design.

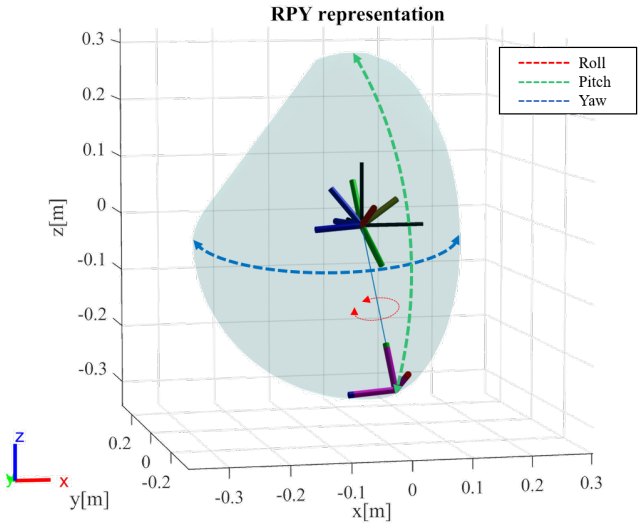

Fig. 3. Graphical representation of the roll, pitch, and yaw axes angles considered to evaluate the spherical joint's internal-external rotation and manipulability within the considered ranges. Roll represents humerus rotation along its axis, pitch represents elevation, and yaw represents horizontal rotation.

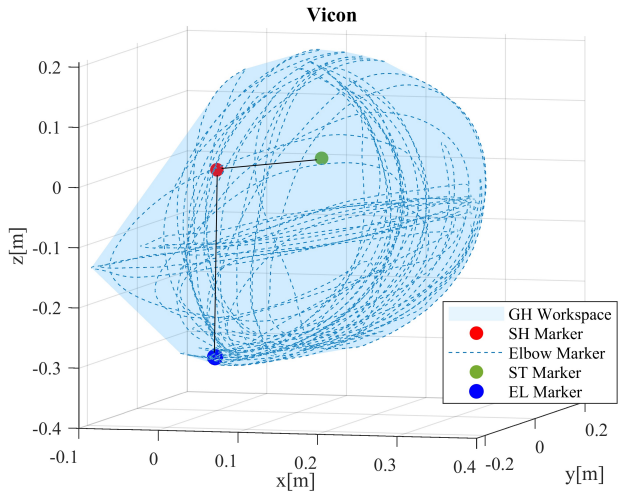

Fig. 4. The figure depicts the positions of three markers on the subject's upper limb: a reference marker on the sternum (green), one marker at the shoulder (red), and one at elbow (blue) level. To calculate the amplitude of abduction and flexion movements, it was necessary to reconstruct the sternum-shoulder segment (from the green to the red marker) and the shoulder-elbow segment (from the red to the blue marker). The gleno-humeral (GH) workspace covered by the healthy individual is illustrated in light blue, along with the trajectory traced by the elbow marker (represented by a blue dash-line). The performed movements aimed to determine the maximum levels of flexion and abduction achievable without involving scapular rhythm.

III. DESIGN

A. Exoskeleton kinematics

The design choice was to propose a 3-DoF RPY wrist instead of the previously adopted 3-DoF Eulerian wrist, to resemble the glenohumeral shoulder joint complex. The developed kinematics structure can be described through the modified Denavit-Hartenberg (mDH) convention [22].

To compute the direct kinematics, the mDH parameters (a, α, d, θ) to define the different homogeneous transformations are reported in Table II.

TABLE II

MDH PARAMETERS FOR THE 6 DOF EXOSKELETON PROTOTYPE.

Link ID	a [m]	α [rad]	d [m]	θ [rad]
1	0	π	0	$0+\theta_1$
2	0	$-\pi/2$	0.009	$\pi/2+\theta_2$
3	0	$-8\cdot\pi/9$	0	$\pi/3+\theta_3$
4	0	$59\cdot\pi/180$	0	$-\pi/2+\theta_4$
5	0	$-\pi/3$	0	$0+\theta_5$

The translation t_{12} an t_{23} are intended to be pre-multiplied to the mDH matrices.

$$t_{12} = \begin{bmatrix} 0 \\ 0 \\ -0.173\,\text{m} \\ 1 \end{bmatrix} \quad \text{and} \quad t_{23} = \begin{bmatrix} 0 \\ 0.199\,\text{m} \\ 0.236\,\text{m} \\ 1 \end{bmatrix}$$

The transformation matrices T_{56} and T_{6EE} describe the relation between reference frame 5 and 6 and between reference frame 6 and the end-effector placed at the end of the last link.

$$T_{56} = \begin{bmatrix} -\sin(\theta_6) & -\cos(\theta_6) & 0 & 0 \\ \cos(\theta_6) & -\sin(\theta_6) & 0 & -0.295\,\text{m} \\ 0 & 0 & 1 & 0 \\ 0 & 0 & 0 & 1 \end{bmatrix}$$

$$T_{6EE} = \begin{bmatrix} 1 & 0 & 0 & 0 \\ 0 & 1 & 0 & -0.150\,\text{m} \\ 0 & 0 & 1 & 0.080\,\text{m} \\ 0 & 0 & 1 & 0 \end{bmatrix}$$

The overall transformation between the reference frame and the exoskeleton can be described as:

$$T_{0EE} = T_{01} \cdot T_{12} \cdot T_{23} \cdot T_{34} \cdot T_{45} \cdot T_{56} \cdot T_{6EE} \tag{6}$$

The angles θ_i represent the degrees of freedom (DoF) of the exoskeleton. These rotations are confined within the range of motion (ROM) shown in Table III. They are limited by mechanical stops designed to prevent collisions and ensure user safety.

Joint	Eulerian Wrist ROM [deg]	RPY Wrist ROM [deg]
J3	101	131
J4	95	160
J5	110	172

TABLE III

COMPARISON OF RANGE OF MOTION (ROM) FOR JOINTS IN EULERIAN WRIST AND RPY WRIST

IV. RESULTS

The rigid body trees models for the shoulder joints of both the Float (Eulerian wrist design) and Spherical Float (RPY wrist design) configurations were constructed and analyzed exploiting MATLAB Robotic Toolbox.

A. Kinematics evaluation: workspace

The robot workspaces were simulated by exploiting rigid body tree models. The different combinations of rotations of the J3, J4, and J5 joints (within their respective ranges of motion) were tested to derive the *x, y, z* Cartesian coordinates of the elbow (end-effector), which can be used to compute the workspace surface (Figure 5). These data were then compared with those collected from Vicon analysis of a subject with corresponding anthropometry. The areas for the physiological workspace, as well as for the Eulerian and RPY wrist designs, are reported in Table IV.

B. Kinematics evaluation: internal-external rotation

The assessment of Internal-External rotation shown in Figure 6, leverages the representation introduced by A. H. Stienen and A. Q. Keemink [24]. The evaluation of the humerus rotation range exploits the Roll-Pitch-Yaw (RPY) representation. The range of internal and external rotation is depicted by blue semi-circles, indicating the span between the maximum and minimum roll angles calculated within a

	Eulerian Design	RPY Design	GH+SC (161.5° flex - 151.5° abd)	GH (90° flex - 90° abd)	Vicon
Workspace Area [m^2]	0.219	0.687	0.463	0.137	0.099
% of Covered Vicon Area	67.5%	95.7%	-	-	-

TABLE IV

THE TABLE SHOWS THE COMPUTED SURFACE AREAS COVERED BY THE TWO SPHERICAL JOINT DESIGNS, VICON ANALYSIS, AND THEORETICAL LIMITS BASED ON TYPICAL MAXIMUM AND MINIMUM FLEXION AND ABDUCTION OF A HEALTHY SUBJECT [23]. IT INCLUDES BOTH GLENOHUMERAL AND SCAPULAR COMPLEXES OR RESTRICTED MOVEMENTS MINIMIZING SCAPULAR RHYTHM. ADDITIONALLY, IT ANALYZES HOW MUCH OF THE VICON WORKSPACE IS COVERED BY THE PROPOSED MECHANISM.

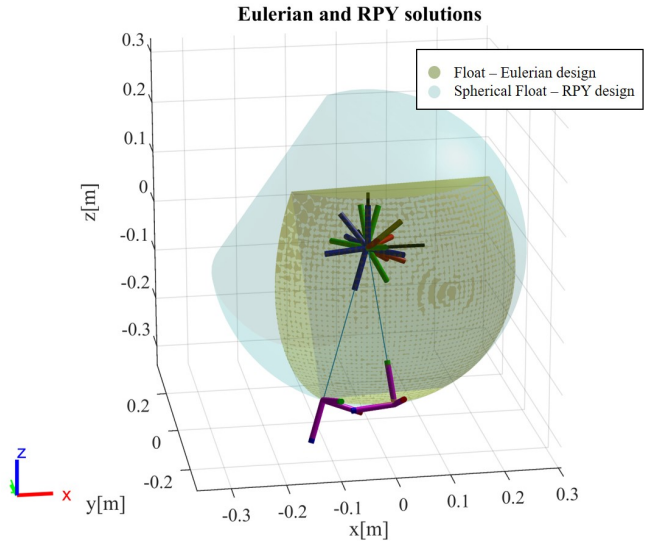

Fig. 5. Workspace evaluation: surfaces covered with the 3-DOF Eulerian and RPY wrist solutions. The rigid body trees of the two designs are reported together with the workspace allowed by the joint range of motion.

specific configuration determined by the yaw (Glenohumeral Horizontal Rotation) and pitch (Glenohumeral Elevation Rotation) coordinates on the planetary.

C. Kinematics evaluation: manipulability

For each joint within its operational range, the manipulability, encompassing accepted Roll-Pitch-Yaw (RPY) combinations, associated with the respective pose was computed.

V. DISCUSSION

The newly proposed shoulder design aims to enable an extension of reachable workspace and to enhance the internal-external rotation performances while guaranteeing the level of manipulability required to facilitate a natural use of the exoskeleton by the patient. We proposed a 3-DoF RPY wrist to resemble the glenohumeral shoulder joint complex. During the design, the range of motion of each joint was chosen to avoid singular configurations that could lead to a decreased manipulability and to maximise the reachable working area (see Table III).

The previous Eulerian wrist solution provided a simpler movement pattern: each exoskeleton joint was taking care of a specific human shoulder movement. However, it suffered from singularities i.e., gimbal lock, in particularly useful configurations of the arm (see Table I).

A reworked kinematic structure for the Float exoskeleton to improve its rehabilitative capabilities was proposed. The 3-DOF RPY (Roll-Pitch-Yaw) design expands the device's overall range of motion, enhancing its ability to cover a wider portion of the physiological range (see Table IV, Figure 5).

Also, the Eulerian design offered a limited internal-external rotation (see Figure 6). By contrast, the new RPY solution offers a larger internal-external rotation (see Figure 6), while also moving the singular configurations away from most of the activities of daily living (Table I).

An analysis was conducted on the reachable workspace surface, comparing the area covered by Eulerian and RPY designs and assessing both results against physiological standard. Biomechanical literature indicates that healthy subjects typically achieve maximum flexion and abduction movements of the glenohumeral joint and scapular complex (GH+SC) on the order of 161.5° and 151.5° respectively [23]. Exploiting this data, the abduction-flexion relation (Figure 7) and consequently, the maximum spherical surface area that can be covered by the joint were estimated (Table IV). Data collected through the Vicon system during shoulder mobilization of a healthy subject (without involving scapular movement) identified the area covered solely by the glenohumeral complex (Figure 4). This was compared to the theoretical area derived from flexion and abduction movements limited to a maximum of 90° to limit the involvement of the scapular complex.

To assess the surfaces covered by the proposed kinematics, a surface integral was performed. The regions identified by the abduction-flexion relationship were translated into the spherical surface integral domain. These areas were then divided and approximated into rectangles, as shown in Figure 8. The integration limits are thus determined by the vertices of the identified rectangles. The computed surfaces are reported in Table IV.

Analysis revealed that - while the Eulerian design covers approximately 50% of the expected area under GH+SC conditions - the RPY joint maximizes the workspace, allowing exploration of motion ranges inaccessible with the Eulerian joint. The RPY area is increased by approximately 3 times compared to the area of the Eulerian solution, facilitating optimized coverage of physiological movement. However, there is still room for improvement, as a portion of the Vicon area (Figure 7) is not covered. This uncovered area, with a size of $\sigma = 0.00422m^2$, constitutes 4.26% of the overall recorded area.

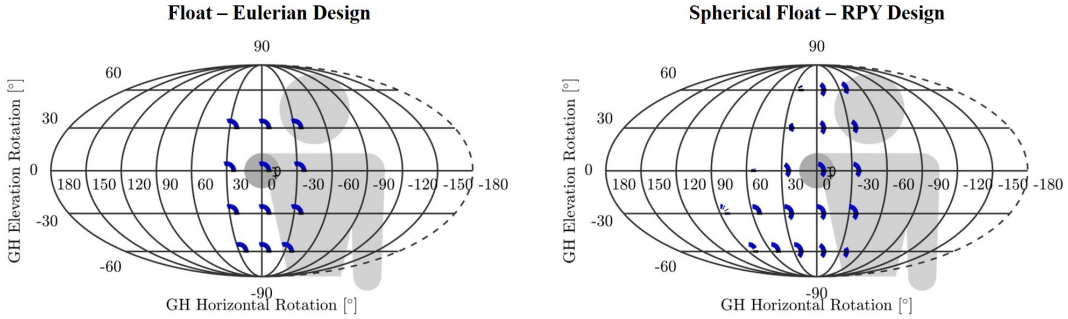

Fig. 6. Comparison between the internal-external rotation achievable with the 3-DOF Eulerian and RPY wrist solutions within the analyzed range. The intra-extra rotation is quantified by the blue semi-circles, representing the range between maximum and minimum roll angles computed in that configuration, identified by yaw (GH Horizontal Rotation) and pitch (GH Elevation Rotation) coordinates on the planetary. This visualization method is recommended by A. H. Stienen and A. Q. Keemink in [24].

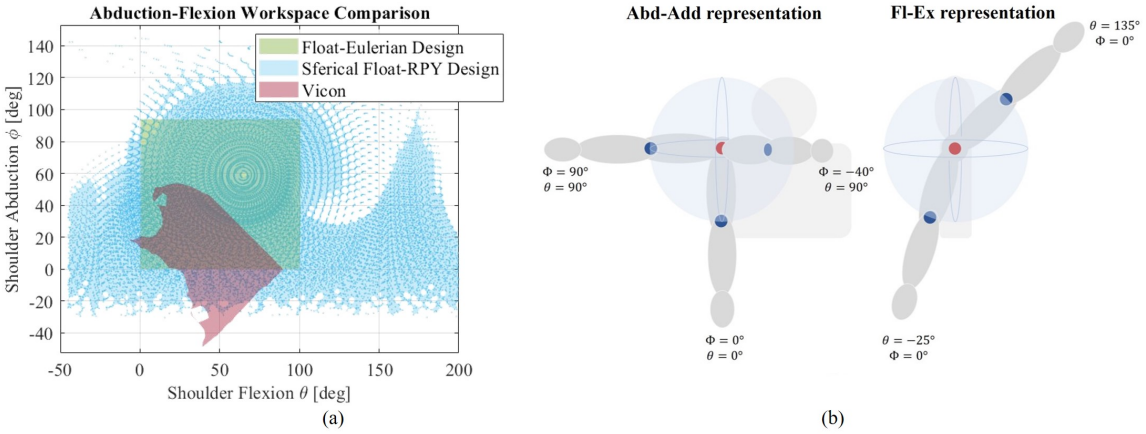

Fig. 7. The figure (a) depicts the relationship between the achieved angles of abduction and flexion in the Eulerian and RPY design, and during the subject test with Vicon capture. The plots illustrate which angle of abduction is attainable at a certain angle of flexion. Figure (b) shows some reference configurations identified by flexion-abduction angles: at 0° fexion - 0° abduction, the arm is considered relaxed along the body. Negative values of θ represent shoulder extension (meaning exploring the space behind the back), negative abduction represents the arm closing towards the counter-side shoulder.

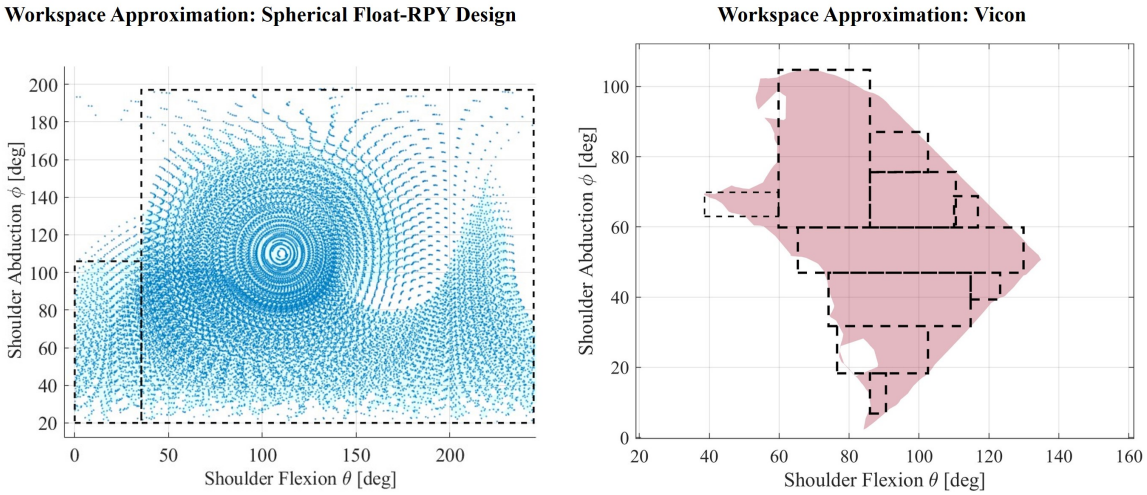

Fig. 8. For the surface analysis, to identify the integration limits, it's useful to divide the represented regions into rectangular sections and then sum the various surface integrals. The figure reports how the RPY and Vicon abduction-flexion areas have been approximated. The surfaces were mapped into the correct domain where the spherical surface integration is defined.

The results enabled a comparison of the performances of the proposed designs in covering the glenohumeral joint

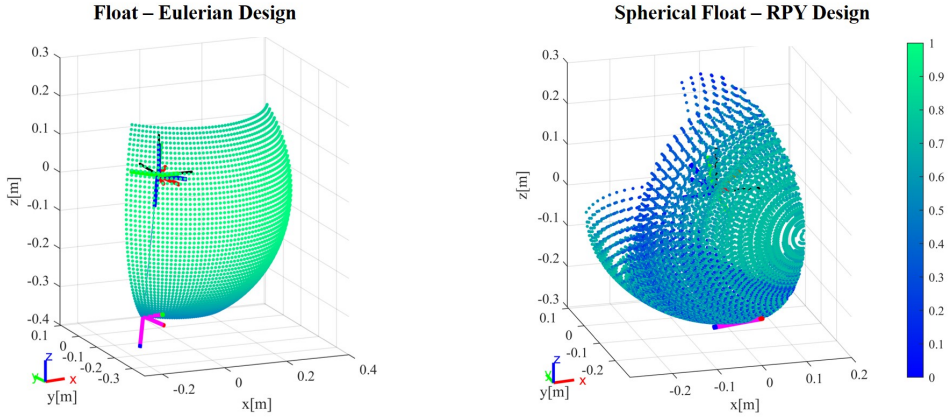

Fig. 9. Manipulability study and representation. Comparison between the two different kinematics: all the combination of joints values inside the joints working range, (resulting in RPY considered combinations), were used to compute the manipulability associated to that pose.

workspace. Referring to Figure 7, where overlaid graphs depict the relationship between abduction and flexion angles, a resting position is used as a reference, where the arm is extended along the body, indicating null flexion and abduction. Positive θ angles correspond to shoulder flexion, while negative angles indicate shoulder extension (ranging from the resting position to exploring the negative space behind the frontal plane). Positive abductions angles Φ, entail an opening of the angle formed between the trunk and arm, while negative abductions involve movements of external rotation or reaching of the contralateral shoulder, with the elbow brought in front of the trunk. The analysis reveals that both the RPY solution and the Eulerian solution cover a more extensive space compared to that detected with Vicon acquisitions. This feature, coupled with the scapular joint interaction of the exoskeletons, is then leveraged to recreate a correct physiological movement of the scapular rhythm and the glenohumeral joint.

One notable advantage of the RPY wrist solution is its ability to explore previously unreachable negative space (see Figure 7), namely including areas behind the frontal plane. This capability is essential for performing activities of daily living, such as reaching behind the head, reaching a back-pocket, or extending the shoulder. Additionally, the RPY design facilitates shoulder rotation around the arm's longitudinal axis without the need for a dedicated joint (J5 in Float), thanks to the composite movement of the spherical wrist (J3, J4, J5 in Spherical Float).

The internal-external rotation was analyzed, considering the neutral position (null rotation) of the upper limb as extended forward (palm facing downward). Referring to Figure 6, for example, at yaw (GH Horizontal Rotation) and pitch (GH Elevation Rotation) coordinates of 0°, a roll (internal-external rotation) ranging from 44° of internal rotation to 88° of external rotation is allowed. The analysis of internal-external rotation shows that this movement, thanks to the RPY wrist design, can be performed across a wider area of the workspace, especially compared to the Float design. Specifically, the new kinematics enable the execution of the movement within regions defined by yaw values between -30° and 30° and pitch values between 30° and 60°, as well as yaw values between 60° and 90° and pitch values between -60° and 0°, which were previously not achievable with the Eulerian wrist design. However, this increased flexibility comes with a trade-off: there is a reduction in the range of roll (internal-external rotation) at certain configurations compared to the Float design, such as at yaw values between -30° and 30° and pitch 30°. Comparing Eulerian and RPY wrists, the maximum internal and external rotations are, respectively, 2° and 110° ($\pm$56 considering a resting position of the arm opened by 30° with respect to the frontal plane) for the Eulerian design, and 45° and 90° for the RPY solution.

The study of manipulability reveals that the gains in terms of workspace and internal-external rotation result in a decrease in the usability of the device, particularly when comparing the Float design (Eulerian wrist), where manipulability ranged between 0.53 and 1, to the Spherical Float design (RPY wrist), where manipulability varies between 0.014 and 0.74 (Figure 9). In the RPY solution, the lower manipulability is observed in regions reachable with configurations close to singularities, where changing the pose of the end-effector is a challenging task to be achieved.

Table V presents the ROM covered by various exoskeletons: Harmony [18], AnyExo [17], Float [13], and SphericalFloat.

	Harmony [°]	AnyExo2.0 [°]	Float [°]	Sph.Float [°]
Flex	160	140	100	**200**
Ext	-45	-20	0	**-45**
Abd	118	135	95	**140**
Add	-60	0	0	**-25**
In.Rot.	-130	-80	-56	**-45**
Ex.Rot.	79	130	56	**90**

TABLE V

COMPARISON OF THE MAXIMUM RANGE OF MOTION (ROM) ATTAINABLE FOR DIFFERENT MOVEMENTS BY DIFFERENT EXOSKELETONS: [18], [17], [13]

This comparison serves to evaluate the performance of our proposed spherical joint design against competing devices. As indicated, the RPY solution represents an advancement over the Eulerian joint design featured in Float, enabling broader movements, including adduction and extension, and notably enhancing external rotation capabilities. In comparison to Harmony, our proposed RPY solution aligns well with extension performance, while also improving flexion, abduction, and external rotation, albeit with slight limitations in internal rotation and adduction. When compared to AnyExo, our solution demonstrates competitiveness in flexion-extension and abduction.

VI. CONCLUSION

This study introduces a methodology combining reachable workspace, internal-external rotation, and manipulability analysis to assess a robotic rehabilitation device's compatibility with the human body. Results indicate that replacing the Eulerian wrist with an RPY wrist enhances range of motion and adaptability for shoulder rehabilitation, though it slightly reduces overall manipulability. These findings have significant implications for developing more effective and intuitive robotic rehabilitation devices for individuals with shoulder impairments. Future developments will explore different RPY configurations and improve the alignment between human and exoskeleton joints to further enhance the device's rehabilitative capabilities. Plans include conducting evaluation tests of the proposed kinematics through organized clinical trials to gain a deeper understanding of the coupling between the glenohumeral and scapular joints with the exoskeleton, and to assess the limitations of such kinematics in mimicking physiological movements.

ACKNOWLEDGMENT

This work was funded by the Istituto Nazionale per l'Assicurazione contro gli Infortuni sul Lavoro (INAIL) under grant agreements "PR19-RR-P2 - RoboGYM and "PR23-RR-P2 - ClinicEXO".

REFERENCES

[1] Nathanael Jarrasse and Guillaume Morel. Connecting a human limb to an exoskeleton. *IEEE Transactions on Robotics*, 28:697–710, 01 2011.

[2] Nives Klopčar and Jadran Lenarčič. Kinematic model for determination of human arm reachable workspace. *Meccanica*, 40(2):203–219, 2005.

[3] J IJspeert, R Lustenhouwer, RM Janssen, and et al. Reachable workspace analysis is a potential measurement for impairment of the upper extremity in neuralgic amyotrophy. *Muscle & Nerve*, 66(3):282–288, 2022.

[4] Stephen J. Housman, Le Vu, Talat Rahman, Rafael J. Sanchez, and David J. Reinkensmeyer. Arm-training with t-wrex after chronic stroke: Preliminary results of a randomized controlled trial. In *Rehabilitation Robotics, 2007. ICORR 2007. IEEE 10th International Conference on*, pages 562–568. IEEE, June 2007.

[5] André Schiele and Frans van der Helm. Kinematic design to improve ergonomics in human machine interaction. *IEEE transactions on neural systems and rehabilitation engineering : a publication of the IEEE Engineering in Medicine and Biology Society*, 14:456–69, 01 2007.

[6] A.S. Niyetkaliyev, S. Hussain, M.H. Ghayesh, and Gursel Alici. Review on design and control aspects of robotic shoulder rehabilitation orthoses. *IEEE TRANSACTIONS ON HUMAN-MACHINE SYSTEMS*, 47(6):1134–1145, dec 2017.

[7] R. Gopura and K. Kiguchi. Mechanical designs of active upper-limb exoskeleton robots: State-of-the-art and design difficulties. *IEEE 11th International Conference on Rehabilitation Robotics Kyoto International Conference Center*, pages 178–187, jul 2009.

[8] Randa Mallat, Mohamad Khalil, Gentiane Venture, Vincent Bonnet, and Samer Mohammed. Human-exoskeleton joint misalignment: A systematic review. pages 1–4, 10 2019.

[9] Yves Zimmermann, Jaeyong Song, Cédric Deguelle, Julia Läderach, Lingfei Zhou, Marco Hutter, Robert Riener, and Peter Wolf. Human–robot attachment system for exoskeletons: Design and performance analysis. *IEEE Transactions on Robotics*, 39(4):3087–3105, 2023.

[10] Ajay Seth, Ricardo Matias, António P Veloso, and Scott L Delp. A biomechanical model of the scapulothoracic joint to accurately capture scapular kinematics during shoulder movements. *PLOS ONE*, 11(1):e0141028, 2016.

[11] Ahmet E. Engin and S. T. Tümer. Three-dimensional kinematic modelling of the human shoulder complex—part i: Physical model and determination of joint sinus cones. *Journal of Biomechanical Engineering*, 111(2):107–112, May 1989.

[12] Oliver Rettig, Laetitia Fradet, Philip Kasten, Patric Raiss, and Sebastian I. Wolf. A new kinematic model of the upper extremity based on functional joint parameter determination for shoulder and elbow. *Gait & Posture*, 30(4):469–476, 2009.

[13] S. Buccelli, F. Tessari, F. Fausto, L. De Guglielmo, and G. Capitta et Al. A gravity-compensated upper-limb exoskeleton for functional rehabilitation of the shoulder complex. *Applied Sciences*, 12(7), 2022.

[14] Kinetec, alex exoskeleton. `http://www.wearable-robotics.com/kinetek/products/alex/`.

[15] Hocoma website. `https://www.hocoma.com/solutions/armeo-power/`.

[16] Zeiaee A., Soltani-Zarrin R., Langari R., and Tafreshi R. Design and kinematic analysis of a novel upper limb exoskeleton for rehabilitation of stroke patients. In *2017 International Conference on Rehabilitation Robotics (ICORR)*, pages 759–764, 2017.

[17] Zimmermann Y., Sommerhalder M., Wolf P., Riener R., and Hutter M. Anyexo 2.0: A fully-actuated upper-limb exoskeleton for manipulation and joint-oriented training in all stages of rehabilitation. *IEEE Transactions on Robotics*, 2023.

[18] Kim B. and Deshpande A. D. An upper-body rehabilitation exoskeleton harmony with an anatomical shoulder mechanism: Design, modeling, control, and performance evaluation. *The International Journal of Robotics Research*, 36:414 – 435, 2017.

[19] Pignolo L., Dolce G., Basta G., Lucca L. F., Serra S., and Sannita W. G. Upper limb rehabilitation after stroke: Aramis a "robo-mechatronic" year=2012, volume=, number=, pages=1410-1414, doi=10.1109/BioRob.2012.6290868. In *2012 4th IEEE RAS and EMBS International Conference on Biomedical Robotics and Biomechatronics (BioRob)*.

[20] Giulia Bodo, Federico Tessari, Stefano Buccelli, and Matteo Laffranchi. A rapid control prototyping and hardware-in-the loop approach for upper limb robotic exoskeletons control. *Applied Sciences*, 14(5), 2024.

[21] Young Mi Lee, Seung Lee, Kyung Eun Uhm, Gregor Kurillo, Ji-Won Han, and Jong Dae Lee. Upper limb three-dimensional reachable workspace analysis using the kinect sensor in hemiplegic stroke patients: A cross-sectional observational study. *American Journal of Physical Medicine & Rehabilitation*, 99(5):397–403, 2020.

[22] Chennakesava Reddy A. Difference between denavit - hartenberg (d-h) classical and modified conventions for forward kinematics of robots with case study. *International Conference on Advanced Materials and manufacturing Technologies (AMMT)*, pages 267–286, dec 2014.

[23] Tiffany K Gill, E Michael Shanahan, Graeme R Tucker, Rachelle Buchbinder, and Catherine L Hill. Shoulder range of movement in the general population: age and gender stratified normative data using a community-based cohort. *BMC Musculoskeletal Disorders*, 21(1):676, 2020.

[24] Arno H. A. Stienen and Arvid Q. L. Keemink. Visualization of shoulder range of motion for clinical diagnostics and device development. *2015 IEEE International Conference on Rehabilitation Robotics (ICORR)*, pages 816–821, 2015.